THE JOURNAL OF PHYSICAL CHEMISTRY A

Article

Cite This: J. Phys. Chem. A 2019, 123, 9809−9817

pubs.acs.org/JPCA

Calculation of Chemical Reaction Barrier Heights by Multiconfiguration Pair-Density Functional Theory with Correlated Participating Orbitals

Andrew M. Sand,[†,‡] Katherine M. Kidder,[†] Donald G. Truhlar,[*,†] and Laura Gagliardi[*,†]

[†]Department of Chemistry, Chemical Theory Center, and the Minnesota Supercomputing Institute, The University of Minnesota, Minneapolis, Minnesota 55455, United States

[‡]Department of Chemistry and Biochemistry, Butler University, Indianapolis, Indiana 46208, United States

Supporting Information

ABSTRACT: The accurate description of reaction barrier heights is challenging for quantum mechanical methods due to the need for a balanced treatment of dynamic and static correlation energies because their importance varies during the course of a chemical reaction. While some regions of potential energy surfaces are well-described by a single-reference wave function or by Kohn−Sham density functional theory, in other cases a multireference treatment is needed. For systems with many active electrons, most accurate multireference methods have prohibitive computational scalings with system size. Multiconfiguration pair-density functional theory, MC-PDFT, is a more affordable multireference approach that computes the total electron correlation energy in a single step by using the multiconfiguration kinetic energy, density, and on-top pair density and an on-top density functional. In this work, we apply MC-PDFT to a benchmark database (DBH24/18) of 24 diverse reaction barrier heights. We explore the role of active space and basis set selection on the performance of MC-PDFT. We find that MC-PDFT is able to calculate reaction barrier heights with a similar accuracy to complete active space second order perturbation theory, CASPT2, but at a lower computational cost, and we find that MC-PDFT is less dependent on basis set selection than CASPT2.

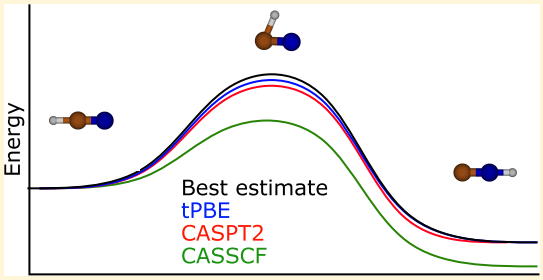

1. INTRODUCTION

The study of chemical reactions by theoretical chemistry generally requires calculating the energies of important points on a Born−Oppenheimer potential energy surface, including minima corresponding to reactants and products and saddle points corresponding to transition structures. In order to obtain accurate energies, theoretical methods must be employed that are capable of recovering both dynamic and static correlation energy.[1] For this reason, multireference methods are often employed.[2−5] In most such approaches, a multiconfiguration self-consistent field (MCSCF)[6−11] step is performed first to serve as a reference calculation to recover predominantly static correlation energy, and an additional calculation is performed to recover primarily dynamic correlation energy. Some methods commonly used include complete active space second-order perturbation theory (CASPT2),[12] multireference Møller−Plesset second-order perturbation theory (MRMP2),[13−15] or one of their variants and multireference configuration-interaction (MRCI).[16,17] One drawback of these methods is that the cost of the post-SCF step often scales poorly with system size, and thus, applications of these methods are often limited to systems of small-to-medium size.

A newer approach to the handling of multiconfigurational systems is multiconfiguration pair-density functional theory (MC-PDFT).[18,19] MC-PDFT is a special type of density functional theory that combines advantages from both multiconfiguration wave function theories and traditional Kohn−Sham density functional theory. In an MC-PDFT calculation, one evaluates an on-top density functional using the density and on-top pair density of a MCSCF wave function. The unpartitioned electron correlation energy is computed in a noniterative post-SCF step by using the MCSCF kinetic energy, the classical Coulomb contributions, and the on-top density functional. Any method providing one- and two-electron reduced density matrices can be used as a starting point for a subsequent MC-PDFT energy calculation. While CASSCF reference wave functions have been most commonly used, restricted active space,[20−22] generalized active space,[9] and density matrix renormalization group[23,24] wave functions have also been used in conjunction with MC-PDFT.

MC-PDFT has several computational advantages over other post-MCSCF methods. First, the computational cost of the evaluation of the on-top density functional scales modestly as N^4 with the number of active orbitals, meaning the cost of the post-SCF step does not usually contribute substantially to the

Received: August 26, 2019
Revised: September 30, 2019
Published: October 14, 2019

DOI: 10.1021/acs.jpca.9b08134
J. Phys. Chem. A 2019, 123, 9809−9817

Table 1. Active Space Descriptions for Each Reaction in the DBH24 Database for the *nom*-CPO and *mod*-CPO Methodologies

reaction	*nom*-CPO MOs	*nom*-CPO (*e*,*o*)	*mod*-CPO MOs	*mod*-CPO (*e*,*o*)
R1: OH + CH_4 → CH_3 + H_2O	$\sigma_{OH}\|\sigma_{CH}$, $\sigma^*_{OH}\|\sigma^*_{CH}$, $2p_{zO}\|2p_{zC}$ (SOMO)	(3,3)	$\sigma_{OH}\|\sigma_{CH}$, $\sigma^*_{OH}\|\sigma^*_{CH}$, $2p_{zO}\|2p_{zC}$ (SOMO), $2p_{xO}$, $2p_{yO}$, $2p'_{xO}$, $2p'_{yO}$	(7,7)
R2: H + OH → O + H_2	$\sigma_{OH}\|\sigma_{HH}$, $\sigma^*_{OH}\|\sigma^*_{HH}$, $2p_{xO}$ (SOMO), $1s_H\|2p_{zO}$ (SOMO)	(4,4)	$\sigma_{OH}\|\sigma_{HH}$, $\sigma^*_{OH}\|\sigma^*_{HH}$, $2p_{xO}$ (SOMO), $1s_H\|2p_{zO}$ (SOMO), $2p_{yO}$, $2p'_{yO}$	(6,6)
R3: H + H_2S → H_2 + HS	$\sigma_{SH}\|\sigma_{HH}$, $\sigma^*_{OH}\|\sigma^*_{HH}$, $1s_H\|3p_{zS}$ (SOMO)	(3,3)	$\sigma_{SH}\|\sigma_{HH}$, $\sigma^*_{OH}\|\sigma^*_{HH}$, $1s_H\|3p_{zS}$ (SOMO), $3p_{xS}$, $3p_{yS}$, $3d_{xyS}$, $3d_{(x^2-y^2)S}$	(7,7)
R4: H + N_2O → N_2 + OH	$2p_{xO}$, $2p_{yO}$, $2p_{xN_a}$, $2p_{yN_a}$, $2p_{xN_b}$, $2p_{yN_b}$, $2p'_{xO}$, $2p'_{yO}$, $1s_H\|2p_{zO}$ (SOMO), $\sigma_{NO}\|\sigma_{NN}$, $\sigma^*_{NO}\|\sigma^*_{NN}$	(11,11)	$2p_{xO}$, $2p_{yO}$, $2p_{xN_a}$, $2p_{yN_a}$, $2p_{xN_b}$, $2p_{yN_b}$, $2p'_{xO}$, $2p'_{yO}$, $1s_H\|2p_{zO}$ (SOMO), $\sigma_{NO}\|\sigma_{NN}$, $\sigma^*_{NO}\|\sigma^*_{NN}$	(11,11)
R5: H + ClH → HCl + H	σ_{ClH}, σ^*_{ClH}, $1s_H$	(3,3)	σ_{ClH}, σ^*_{ClH}, $1s_H$, $3p_{yCl}$, $3d_{xyCl}$, $3d_{(x^2-y^2)Cl}$	(7,7)
R6: CH_3 + FCl → CH_3F + Cl	$\sigma_{FCl}\|\sigma_{CF}$, $\sigma^*_{FCl}\|\sigma^*_{CF}$, $2p_{zC}\|3p_{zCl}$ (SOMO)	(3,3)	$\sigma_{FCl}\|\sigma_{CF}$, $\sigma^*_{FCl}\|\sigma^*_{CF}$, $2p_{zC}\|3p_{zCl}$ (SOMO), $2p_{xF}$, $2p_{yF}$, $2p'_{xF}$, $2p'_{yF}$, $3p_{xCl}$, $3p_{yCl}$, $3d_{xyCl}$, $3d_{(x^2-y^2)Cl}$	(11,11)
R7: Cl^- ··· CH_3Cl → $ClCH_3$ ··· Cl^-	σ_{CCl}, σ^*_{CCl}, $3p_{zCl}$, $3d_{z^2Cl}$	(4,4)	σ_{CCl}, σ^*_{CCl}, $3p_{zCl}$, $3d_{z^2Cl}$ $3p_{xCl_a}$, $3p_{xCl_b}$, $3p_{yCl_a}$, $3p_{yCl_b}$, $3d_{xzCl_a}$, $3d_{xzCl_b}$, $3d_{yzCl_a}$, $3d_{yzCl_b}$	(12,12)
R8: F^- ··· CH_3Cl → FCH_3 ··· Cl^-	$\sigma_{CCl}\|\sigma_{CF}$, $\sigma^*_{CCl}\|\sigma^*_{CF}$, $2p_{zF}\|3p_{zCl}$, $2p'_{zF}\|3d_{z^2Cl}$	(4,4)	$\sigma_{CCl}\|\sigma_{CF}$, $\sigma^*_{CCl}\|\sigma^*_{CF}$, $2p_{zF}\|3p_{zCl}$, $2p'_{zF}\|3d_{z^2Cl}$, $3p_{xCl}$, $2p_{xF}$, $3p_{yCl}$, $2p_{yF}$, $3d_{xzCl}$, $2p'_{xF}$, $3d_{yzCl}$, $2p'_{yF}$	(12,12)
R9: OH^- + CH_3F → $HOCH_3$ + F^-	$\sigma_{CF}\|\sigma_{CO}$, $\sigma^*_{CF}\|\sigma^*_{CO}$, $2p_{zO}\|2p_{zF}$, $2p'_{zO}\|2p'_{zF}$	(4,4)	$\sigma_{CF}\|\sigma_{CO}$, $\sigma^*_{CF}\|\sigma^*_{CO}$, $2p_{zO}\|2p_{zF}$, $2p'_{zO}\|2p'_{zF}$, $2p_{xF}$, $2p_{xO}$, $2p_{yF}$, $2p_{yO}$, $2'p_{xF}$, $2p'_{xO}$, $2p'_{yF}$, $2p'_{yO}$	(12,12)
R10: H + N_2 → HN_2	$2p_{zN_a}\|\sigma_{NH}$, $2p_{zN_b}$, $1s_H\|\sigma^*_{NH}$	(3,3)	$2p_{zN_a}\|\sigma_{NH}$, $2p_{zN_b}$, $1s_H\|\sigma^*_{NH}$, $2\pi_{xNN}$, $2\pi_{yNN}$, $2\pi^*_{xNN}$, $2\pi^*_{yNN}$	(7,7)
R11: H + C_2H_4 → CH_3CH_2	$2p_{zC_a}\|\sigma_{CH}$, $2p_{zC_b}$, $1s_H\|\sigma^*_{CH}$	(3,3)	$2p_{zC_a}\|\sigma_{CH}$, $2p_{zC_b}$, $1s_H\|\sigma^*_{CH}$	(3,3)
R12: HCN → HNC	$\sigma_{CH}\|\sigma_{NH}$, $\sigma^*_{CH}\|\sigma^*_{NH}$, $2p_{xC}$, $2p_{yC}$, $2p_{xN}$, $2p_{yN}$, $2p'_{xC}$, $2p'_{yC}$, $2p'_{xN}$, $2p'_{yN}$	(10,10)	$\sigma_{CH}\|\sigma_{NH}$, $\sigma^*_{CH}\|\sigma^*_{NH}$, $2p_{xC}$, $2p_{yC}$, $2p_{xN}$, $2p_{yN}$, $2p'_{xC}$, $2p'_{yC}$, $2p'_{xN}$, $2p'_{yN}$	(10,10)

overall cost of the calculation.[25] Second, the on-top density functional calculation depends only on the electron density and on-top pair density and the magnitudes of their gradients, which are easily easily obtainable from the one- and two-body reduced density matrices, and it does not require any other information about the wave function. This enables the straightforward use of the MC-PDFT framework with a diverse variety of reference calculations, such as density matrix renormalization group (DMRG)[26] and variational 2-RDM methods.[27,28] Third, all electron correlation is computed in one shot, unlike CASPT2 which computes external correlation on top of the CASSCF calculation of internal correlation. With the addition of state-interaction pair-density functional theory,[29] locations of the potential energy surface with strong state interactions, such as avoided crossings or conical intersections, can be probed using the PDFT framework as an alternative to quasidegenerate perturbation methods, including QD-NEVPT2,[30] XMCQDPT,[31] XMS-CASPT2,[32] or DMRG-XMS-CASPT2.[33]

In the calculation of reaction barrier heights, the biggest challenge is the characterization of the transition state, which sometimes exhibits effects of strong correlation, making it a challenge to accurately predict the electronic energy and molecular geometry at this point. The recent development of analytic gradients for CAS-PDFT[34] has enabled faster determination of minimum-energy and transition state structures.

The underlying reference CASSCF calculation requires the selection of an active space. Active spaces must conform to the size limitations of the affordability of the corresponding CASSCF calculation (with conventional CASSCF algorithms, this means no larger than 18 active electrons distributed in 18 active orbitals, although recent advances have increased the possible active space size), and they should contain the orbitals "participating" in the chemical process of interest. For the reactions studied in this manuscript, we employ the correlated participating orbitals (CPO) scheme.[35] The CPO scheme, originally developed in the context of providing a multi-configurational theoretical model chemistry,[35−39] gives a framework both to keep the size of the active space manageable and to maintain a balanced description of the orbitals changing the most in the chemical reaction. In this work, we apply MC-PDFT in conjunction with CPO schemes to the DBH24/18 database, which is an update[40] of the original[41] DBH24 database, and it consists of a representative set of 24 barrier heights (forward and reverse reactions) for 12 diverse reactions, including hydrogen transfer reactions, heavy atom transfer reactions, S_N2 reactions, dissociation and addition reactions, and rearrangement reactions.

The purpose of this paper is to evaluate the accuracy of MC-PDFT in determining reaction barrier heights and compare these results to both experimental and CASPT2 calculations. We benchmark our results against the DBH24/18 database. Additionally, we aim to evaluate the characteristics of the transition state structures and explore the effect of the active space size and basis set on the quality of MC-PDFT results. To carry out these objectives, we identify the participating and correlating orbitals using two different schema. In the nominal (*nom*-CPO) scheme, the participating orbitals are selected to be those that describe bonds (π or σ) that are broken or formed during the reaction; any singly occupied orbital is also included. For each participating bonding orbital, a correlating orbital consisting of the σ^* or π^* bond is additionally included in the active space definition. No additional correlating orbital is included for singly occupied orbitals. In the moderate (*mod*-CPO) scheme, the orbitals included in the active space are those included in the *nom*-CPO scheme as well as p orbitals containing lone pairs geminal to the bonds that are either broken or formed; additionally, a correlating orbital is included for each lone-pair p orbital. For 2p lone pair orbitals, the correlating orbital is a 2p′ orbital, and for 3p lone pair orbitals, the correlating orbital is chosen to be an orbital with mixed 3p′/3d character. These schema allow for consistent active space descriptions across all molecular geometries of interest (reactants, transition states, and products) and allow for an unbiased calculation of the forward and reverse reaction barrier

DOI: 10.1021/acs.jpca.9b08134
J. Phys. Chem. A 2019, 123, 9809−9817

Table 2. Forward and Reverse Barrier Heights for the DBH24 Database Determined with the *nom*-CPO Scheme[a]

		$V_f^{\ddagger}$				$V_r^{\ddagger}$			
	(e,o)	CASSCF	CASPT2	tPBE	best est.[48]	CASSCF	CASPT2	tPBE	best est.[48]
R1	(3,3)	28.54	4.63	4.60	6.3	28.47	16.63	18.57	19.5
R2	(4,4)	16.90	11.87	11.03	10.9	28.69	15.79	8.86	13.2
R3	(3,3)	11.74	5.96	3.82	3.9	25.19	18.36	14.10	17.2
R4	(11,11)	30.21	19.84	17.33	17.7	104.75	86.46	71.03	82.6
R5	(3,3)	29.59	22.75	17.09	17.8	29.59	22.75	17.09	17.8
R6	(3,3)	9.64	3.30	3.62	7.1	63.26	67.19	63.66	59.8
R7	(4,4)	19.79	15.80	12.00	13.5	19.79	15.80	12.00	13.5
R8	(4,4)	4.65	5.76	2.42	3.5	41.06	28.53	27.84	29.6
R9	(4,4)	5.66	−4.06	−3.40	−2.7	27.15	19.76	19.84	17.6
R10	(3,3)	29.04	17.18	13.5	14.6	7.33	11.34	14.27	10.9
R11	(3,3)	8.10	3.81	4.04	2.0	38.51	40.96	43.22	42.0
R12	(10,10)	18.51	27.92	30.08	33.0	39.30	43.61	45.39	48.1

[a]The maug-cc-pVDZ basis set is used. Values are given in kcal/mol.

heights. Explicit specifications for each reaction and each CPO scheme are given in Table 1.

2. THEORY

2.1. MC-PDFT Theory. In an MC-PDFT calculation, the energy is expressed as[18]

$$E_{\mathrm{PDFT}} = V_{\mathrm{nn}} + \sum_{pq} h_{pq} D_{pq} + \frac{1}{2} \sum_{pqst} g_{pqst} D_{pq} D_{st} + E_{\mathrm{ot}}[\rho, \Pi, \rho', \Pi'] \quad (1)$$

where V_{nn} is the nuclear repulsion energy, h_{pq} and g_{pqst} are the one- and two-electron integrals

$$h_{pq} = \int \phi_p^*(\mathbf{r}) h(\mathbf{r}) \phi_q(\mathbf{r})\, \mathrm{d}\mathbf{r} \quad (2)$$

$$g_{pqst} = \int\int \phi_s^*(\mathbf{r}_1) \phi_t(\mathbf{r}_1) \frac{1}{|\mathbf{r}_1 - \mathbf{r}_2|} \phi_p^*(\mathbf{r}_2) \phi_q(\mathbf{r}_2)\, \mathrm{d}\mathbf{r}_1\, \mathrm{d}\mathbf{r}_2 \quad (3)$$

h is the sum of the kinetic energy and nuclear attraction operators, and D_{pq} and d_{pqst} are the one-body and two-body density matrices

$$D_{pq} = \langle \psi | \hat{E}_{pq} | \psi \rangle \quad (4)$$

$$d_{pqst} = \frac{1}{2} \langle \psi | \hat{e}_{pqst} | \psi \rangle \quad (5)$$

where the one- and two-body excitation operators are given as

$$\hat{E}_{pq} = \sum_{\sigma} \hat{a}_{p\sigma}^{\dagger} \hat{a}_{q\sigma} \quad (6)$$

$$\hat{e}_{pqst} = \hat{E}_{pq} \hat{E}_{st} - \delta_{qs} \hat{E}_{pt} \quad (7)$$

where σ indicates α or β spin, and E_{ot} is the on-top density functional with a dependence on the electronic density ρ and the on-top pair density Π

$$\rho(\mathbf{r}) = \sum_{pq} \phi_p(\mathbf{r}) \phi_q(\mathbf{r}) D_{pq} \quad (8)$$

$$\Pi(\mathbf{r}) = \sum_{pqst} \phi_p(\mathbf{r}) \phi_q(\mathbf{r}) \phi_s(\mathbf{r}) \phi_t(\mathbf{r}) d_{pqst} \quad (9)$$

as well as the magnitudes of their gradients

$$|\nabla \rho(\mathbf{r})| = \left| \sum_{pq} (\nabla \phi_p(\mathbf{r}) \phi_q(\mathbf{r}) + \phi_p(\mathbf{r}) \nabla \phi_q(\mathbf{r})) D_{pq} \right| \quad (10)$$

$$|\nabla \Pi(\mathbf{r})| = \Big| \sum_{pqst} (\nabla \phi_p(\mathbf{r}) \phi_q(\mathbf{r}) \phi_s(\mathbf{r}) \phi_t(\mathbf{r}) + \phi_p(\mathbf{r}) \nabla \phi_q(\mathbf{r}) \phi_s(\mathbf{r}) \phi_t(\mathbf{r}) + \phi_p(\mathbf{r}) \phi_q(\mathbf{r}) \nabla \phi_s(\mathbf{r}) \phi_t(\mathbf{r}) + \phi_p(\mathbf{r}) \phi_q(\mathbf{r}) \phi_s(\mathbf{r}) \nabla \phi_t(\mathbf{r})) d_{pqst} \Big| \quad (11)$$

The MC-PDFT method can be applied with any reference wave function for which the one- and two-body density matrices are available, but in this work, we only consider CASSCF reference wave functions.

3. METHODS

The DBH24 database consists of 12 reactions. Reactions **R1**−**R3** are hydrogen transfer reactions, reactions **R4** and **R12** are rearrangements involving multiple bonds, **R5** and **R6** are heavy-atom transfer reactions, reactions **R7**−**R9** are S_N2 reactions, and reactions **R10** and **R11** are association reactions. The active spaces used for each optimization, consistent with either the *nom*-CPO or *mod*-CPO schemes, are given in Table 1. In the definitions of the participating orbitals, a vertical line is used between the orbital for the reactant species (left side) and the corresponding product orbital (right side) for orbitals that change character throughout the reaction. The z-axis is defined to coincide with the direction of bond breaking or forming and the x-axis is defined to be perpendicular to the plane containing the three atoms most closely associated with the bond rearrangement or addition.

All of our CASSCF, CASPT2, and MC-PDFT calculations are nonrelativistic, but the experimental results that we use for benchmark comparison include spin−orbit coupling, a relativistic effect. In order to account for this difference, we add spin−orbit energies for reagents that have nonzero spin−orbit energy contributions. The species for which spin−orbit energy is added and their values (in kcal/mol) are as follows: OH (−0.20),[42] SH (−0.54),[42] and Cl (−0.84).[43] Energy contributions from spin−orbit effects at the saddle points are assumed to be negligible.[44]

DOI: 10.1021/acs.jpca.9b08134
J. Phys. Chem. A 2019, 123, 9809−9817

Table 3. Forward and Reverse Barrier Heights for the DBH24 Database Determined with the *nom*-CPO Scheme[a]

		$V_f^{\ddagger}$				$V_r^{\ddagger}$			
	(*e*,*o*)	CASSCF	CASPT2	tPBE	best est.[48]	CASSCF	CASPT2	tPBE	best est.[48]
R1	(3,3)	28.48	6.09	4.85	6.3	29.66	20.34	20.47	19.5
R2	(4,4)	17.49	11.89	11.59	10.9	29.26	14.48	9.59	13.2
R3	(3,3)	12.22	5.13	4.38	3.9	25.87	17.99	15.41	17.2
R4	(11,11)	31.27	19.44	17.77	17.7	103.18	86.25	69.63	82.6
R5	(3,3)	29.17	19.76	17.1	17.8	29.17	19.76	17.1	17.8
R6	(3,3)	14.74	6.65	6.90	7.1	65.43	66.17	62.08	59.8
R7	(4,4)	23.28	13.96	8.04	13.5	23.28	13.96	8.04	13.5
R8	(4,4)	5.08	4.26	2.50	3.5	43.13	29.31	28.29	29.6
R9	(4,4)	8.21	−4.28	−2.50	−2.7	26.65	16.01	18.42	17.6
R10	(3,3)	29.50	15.54	13.75	14.6	6.88	12.42	14.31	10.9
R11	(3,3)	8.10	2.72	3.99	2.0	38.45	41.44	43.03	42.0
R12	(10,10)	19.93	29.71	31.11	33.0	40.29	44.89	46.19	48.1

[a]The maug-cc-pVTZ basis set is used. Values are given in kcal/mol.

Table 4. Forward and Reverse Barrier Heights for the DBH24 Database Determined with the *mod*-CPO Scheme[a]

		$V_f^{\ddagger}$				$V_r^{\ddagger}$			
	(*e*,*o*)	CASSCF	CASPT2	tPBE	best est.[48]	CASSCF	CASPT2	tPBE	best est.[48]
R1	(7,7)	14.14	7.96	4.20	6.3	31.00	18.59	12.60	19.5
R2	(6,6)	18.82	11.32	7.22	10.9	21.95	15.63	9.43	13.2
R3	(7,7)	32.51	5.77	3.14	3.9	20.07	18.12	15.04	17.2
R4	(11,11)	30.21	19.84	17.33	17.7	104.75	89.06	71.03	82.6
R5	(7,7)	36.29	23.21	12.11	17.8	36.29	23.21	12.11	17.8
R6	(11,11)	12.66	2.83	1.79	7.1	72.42	61.99	55.80	59.8
R7	(12,12)	16.68	15.73	13.54	13.5	16.68	15.73	13.54	13.5
R8	(12,12)	5.14	5.52	3.35	3.5	32.85	35.76	41.95	29.6
R9	(12,12)	2.49	−1.20	−2.76	−2.7	23.84	23.19	20.91	17.6
R10	(7,7)	32.44	18.99	14.07	14.6	2.44	10.26	15.60	10.9
R11	(3,3)	8.10	3.81	4.04	2.0	38.51	40.96	43.22	42.0
R12	(10,10)	18.51	27.92	30.08	33.0	39.30	43.61	45.39	48.1

[a]The maug-cc-pVDZ basis set is used. Values are given in kcal/mol.

Table 5. Forward and Reverse Barrier Heights for the DBH24 Database Determined with the *mod*-CPO Scheme[a]

		$V_f^{\ddagger}$				$V_r^{\ddagger}$			
	(*e*,*o*)	CASSCF	CASPT2	tPBE	best est.[48]	CASSCF	CASPT2	tPBE	best est.[48]
R1	(7,7)	14.26	6.17	4.43	6.3	32.53	18.87	14.17	19.5
R2	(6,6)	19.61	11.07	7.95	10.9	22.58	14.19	10.30	13.2
R3	(7,7)	12.85	5.26	3.5	3.9	24.44	17.45	16.46	17.2
R4	(11,11)	31.27	19.44	17.77	17.7	103.18	86.25	69.63	82.6
R5	(7,7)	36.36	24.14	11.31	17.8	36.36	24.14	11.31	17.8
R6	(11,11)	19.14	6.51	4.56	7.1	74.38	64.96	54.24	59.8
R7	(12,12)	17.64	15.31	14.97	13.5	17.64	15.31	14.97	13.5
R8	(12,12)	5.30	4.23	4.96	3.5	36.15	32.03	27.70	29.6
R9	(12,12)	5.47	−2.65	−10.47	−2.7	23.39	18.08	11.00	17.6
R10	(7,7)	32.83	17.51	14.36	14.6	2.15	11.30	15.56	10.9
R11	(3,3)	8.10	2.72	3.99	2.0	38.45	41.44	43.03	42.0
R12	(10,10)	19.93	29.71	31.11	33.0	40.29	44.89	46.19	48.1

[a]The maug-cc-pVTZ basis set is used. Values are given in kcal/mol.

4. COMPUTATIONAL DETAILS

Geometries for reactants, transition structures, and products were independently optimized for each method and each basis set. All MC-PDFT and CASPT2 calculations were performed using OPENMOLCAS.[45] All CASPT2 calculations used the standard ionization potential/electron affinity (IPEA) shift of 0.25 hartees and all orbitals were correlated except 1s orbitals on non-hydrogen atoms. All CASPT2 geometry optimizations employed numerical gradients, and all CASSCF and MC-PDFT[34] geometry optimizatins used analytic gradients. All MC-PDFT calculations used the tPBE on-top functional.[18] All calculations were performed using the maug-cc-pVDZ and maug-cc-pVTZ basis sets.[46,47]

DOI: 10.1021/acs.jpca.9b08134
J. Phys. Chem. A 2019, 123, 9809−9817

Table 6. Mean Signed Errors (MSE) and Mean Unsigned Errors (MUE) (in kcal/mol) for the Forward and Reverse Reactions (24 Barrier Heights) and Only for Exoergic and Symmetric Reactions (12 Barrier Heights)[a]

		nom-CPO			*mod*-CPO		
basis set		CASSCF	CASPT2	tPBE	CASSCF	CASPT2	tPBE
		forward and reverse					
maug-cc-pVDZ	MSE	6.9	0.9	−1.1	7.0	1.6	−1.4
maug-cc-pVTZ	MSE	7.9	0.6	−1.2	7.3	1.2	−2.4
maug-cc-pVDZ	MUE	9.4	2.7	2.2	10.0	3.0	3.4
maug-cc-pVTZ	MUE	10.3	1.5	2.2	10.1	1.9	3.4
maug-cc-pVDZ	minimum	1.1	0.4	0.1	1.6	0.6	0.0
maug-cc-pVTZ	minimum	1.6	0.0	0.2	1.8	0.1	0.1
maug-cc-pVDZ	maximum	22.4	8.2	11.6	28.6	6.2	12.4
maug-cc-pVTZ	maximum	28.6	7.2	13.0	20.6	6.3	13.0
		forward only					
maug-cc-pVDZ	MSE	7.1	0.6	−1.0	8.4	1.2	−1.6
maug-cc-pVTZ	MSE	8.3	0.3	−0.7	7.9	1.0	−1.6
maug-cc-pVDZ	MUE	9.5	2.6	1.3	10.8	2.7	2.0
maug-cc-pVTZ	MUE	10.5	1.2	1.3	10.1	1.7	2.4

[a]The minimum and maximum error magnitudes are given for each set.

5. RESULTS AND DISCUSSION

Tables 2 and 3 provide results for the *nom*-CPO scheme using the maug-cc-pVDZ and maug-cc-pVTZ basis sets, respectively. Tables 4 and 5 provide results for the *mod*-CPO scheme using the maug-cc-pVDZ and maug-cc-pVTZ basis sets, respectively. Both mean signed errors (MSE) and mean unsigned errors (MUE) for each CPO scheme and basis set are given in Table 6.

A good description of dynamic correlation is essential to obtain good values for the barrier heights. This is evident in a comparison of the results obtained using CASSCF to those obtained using CASPT2. CASSCF describes only the internal correlation, which consists of the static correlation and the limited amount of dynamic correlation within the active space, while CASPT2 introduces additional dynamic correlation by perturbatively describing electron excitations into the external space (i.e., the virtual orbital space). MC-PDFT describes all electron correlation in one shot through its on-top density functional. The errors in the CASSCF barrier heights are considerably higher than the errors for CASPT2 and MC-PDFT, and this explicitly illustrates the need for a post-SCF step.

The quality of the basis set has a strong influence on the accuracy of the CASPT2 calculations because it requires a large basis set to adequately represent dynamic correlation in wave function theory. We used two basis sets: the smaller maug-cc-pVDZ basis set and the larger maug-cc-pVTZ basis set. First we examine the effect of the basis set selection on the mean signed errors (MSE) and mean unsigned errors (MUE). For CASPT2, we observe that for the larger basis set, the MUE and MSE decrease significantly relative to the results obtained with the smaller basis set. For CASSCF and tPBE, however, there is no clear trend in the error as the size of the basis set increases. While the results in Table 6 show that the MSE and MUE of CASSCF slightly increase for CASSCF when going from the smaller to larger basis set, for tPBE we generally observe almost no change in the MSE and MUE values for both the *nom*- and *mod* active space selections. One exception to this trend in tPBE results is seen in the *mod*-CPO case, where the MSE value became 0.9 kcal/mol more negative as the basis set was increased. This increase in error stems almost entirely from too-low barrier heights in **R9**. If instead we consider the errors associated with the 48 individual barrier heights calculated (24 for each the *nom*-CPO and *mod*-CPO schemes), we see that increasing the basis set size results in the computed CASPT2 barrier height improving in 40 of the 48 cases, while CASSCF only shows improvement in 15 of the 48 cases, and tPBE does show improvement in 27 of the 48 cases. Interestingly, the improvement or lack thereof in the tPBE barrier heights is not correlated to the improvements in the CASSCF barrier heights.

We have written all the reactions such that for the unsymmetric reactions, the forward direction is the exoergic direction. By Hammond's postulate,[49] the transition state more closely resembles the reactants for an exoergic reaction than for the reverse endoergic one; thus, it should be easier to balance the active space for calculating forward barrier heights than for calculating reverse ones. Consistent with this, Table 6 shows that the errors in CASPT2 and MC-PDFT are smaller if we consider only the forward reactions; the difference in accuracy between the forward and reverse reactions is particularly large for MC-PDFT.

In the calculation of barrier heights and reaction energies, it is important that multireference methods employ a balanced active space for all reactant, product, and transition state calculations. In order to define these active spaces systematically, we have employed the *nom*-CPO and *mod*-CPO schemes. No systematic improvement is seen for any method going from the smaller and less-costly *nom*-CPO scheme to the larger and more-costly *mod*-CPO. This indicates that even a small number of orbitals in the CPO active space is sufficient for a good description of the chemical reactions. This is encouraging because for larger systems affordable active spaces may be closer to the small one in the present systems than to the large ones. Interestingly, we tend to observe a slight decrease in accuracy as we go to the larger active space. While individual reactant/product and transition state energies improve as the size of the active space is increased, the reaction barriers may increase or decrease (and errors may increase or decrease) as the reactant/product and transition state energies are improving at different rates.

The basis set and active space stability of the tPBE results is quite good. The MUE values for tPBE are within approximately 1 kcal/mol of the MUEs of CASPT2 across

DOI: 10.1021/acs.jpca.9b08134
J. Phys. Chem. A 2019, 123, 9809−9817

Table 7. Selected Transition State Bond Distances (Å) Involved in the Bond Breaking/Bond Forming Process[a]

		maug-cc-pVDZ			maug-cc-pVTZ		
	bond	CASSCF	CASPT2	tPBE	CASSCF	CASPT2	tPBE
R1	O−H	1.263	1.215	1.450	1.264	1.359	1.440
	H−C	1.299	1.281	1.167	1.294	1.184	1.162
R2	H−H	0.842	0.912	0.844	0.834	0.890	0.834
	H−O	1.454	1.219	1.356	1.434	1.220	1.335
R3	H−H	1.097	1.162	1.285	1.087	1.168	1.266
	H−S	1.508	1.445	1.420	1.502	1.428	1.413
R4	H−O	1.407	1.454	1.474	1.388	1.435	1.455
	O−N	1.272	1.239	1.225	1.268	1.230	1.222
R5	H−Cl	1.548	1.510	1.507	1.533	1.489	1.489
	H−Cl	1.548	1.510	1.507	1.533	1.489	1.489
R6	C−F	2.149	2.187	2.197	2.095	2.095	2.112
	F−Cl	1.896	1.798	1.749	1.884	1.771	1.743
R7	Cl−C	2.392	2.313	2.318	2.381	2.284	2.305
	Cl−C	2.392	2.313	2.318	2.381	2.284	2.305
R8	F−C	2.091	2.000	2.106	2.079	1.993	2.075
	Cl−C	2.183	2.172	2.087	2.171	2.122	2.095
R9	O−C	2.019	2.013	2.052	1.999	1.979	2.040
	C−F	1.813	1.755	1.729	1.805	1.737	1.732
R10	H−N	1.349	1.440	1.527	1.333	1.446	1.514
	N−N	1.121	1.144	1.127	1.112	1.128	1.115
R11	H−C	1.885	1.986	2.043	1.876	2.004	2.031
	C−C	1.366	1.364	1.351	1.358	1.348	1.341
R12	H−N	1.393	1.400	1.382	1.384	1.385	1.369
	H−C	1.212	1.204	1.218	1.202	1.189	1.208

[a]The *nom*-CPO scheme was used.

Table 8. Selected Transition State Bond Distances (Å) Involved in the Bond Breaking/Bond Forming Process[a]

		maug-cc-pVDZ			maug-cc-pVTZ		
	bond	CASSCF	CASPT2	tPBE	CASSCF	CASPT2	tPBE
R1	O−H	1.332	1.297	1.480	1.333	1.304	1.474
	H−C	1.239	1.229	1.165	1.233	1.216	1.159
R2	H−H	0.816	0.926	0.933	0.806	0.906	0.936
	H−O	1.549	1.205	1.206	1.525	1.204	1.183
R3	H−H	1.089	1.167	1.332	1.073	1.163	1.374
	H−S	1.506	1.444	1.421	1.499	1.428	1.416
R4	H−O	1.407	1.454	1.474	1.388	1.435	1.455
	O−N	1.272	1.239	1.225	1.268	1.230	1.222
R5	H−Cl	1.526	1.509	1.518	1.510	1.495	1.493
	H−Cl	1.526	1.509	1.518	1.510	1.495	1.493
R6	C−F	2.097	2.204	2.309	2.041	2.108	2.200
	F−Cl	1.848	1.799	1.768	1.840	1.774	1.765
R7	Cl−C	2.385	2.314	2.327	2.376	2.285	2.309
	Cl−C	2.385	2.314	2.327	2.376	2.285	2.309
R8	F−C	2.101	2.194	2.059	2.096	1.996	2.023
	Cl−C	2.184	2.145	2.123	2.168	2.112	2.129
R9	O−C	2.053	2.016	2.051	2.030	1.975	2.044
	C−F	1.831	1.752	1.739	1.824	1.738	1.740
R10	H−N	1.282	1.418	1.511	1.267	1.418	1.498
	N−N	1.157	1.144	1.133	1.148	1.129	1.122
R11	H−C	1.885	1.986	2.043	1.876	2.004	2.031
	C−C	1.366	1.364	1.351	1.358	1.348	1.341
R12	H−N	1.393	1.400	1.382	1.384	1.385	1.369
	H−C	1.212	1.204	1.218	1.202	1.189	1.208

[a]The *mod*-CPO scheme was used.

basis sets and active space selections; tPBE is able to obtain satisfactory results even with the smaller basis set and smaller active space.

We now turn to a comparison of MC-PDFT and CASPT2 results for the various reaction types. Errors are listed by reaction type for each possible selection of method, basis set,

DOI: 10.1021/acs.jpca.9b08134
J. Phys. Chem. A 2019, 123, 9809−9817

and CPO scheme are presented in Tables S1−S5 of the Supporting Information. Reactions **R1**−**R3** are hydrogen transfer reactions. The results obtained with the tPBE functional show good agreement with the CASPT2 results. The largest discrepancy between tPBE and CASPT2 results occurs in the reverse reaction **R2**, but this difference diminishes upon using a larger active space (*mod*-CPO) or a larger basis set (maug-cc-pVTZ).

The S_N2 reactions **R7**−**R9** also show generally good agreement between the tPBE results and CASPT2 results, although CASPT2 is slightly less affected by active space size or basis set quality. The tPBE results generally showed small errors with the exception of the reverse reaction **R8** determined using the *mod*-CPO scheme with the maug-cc-pVDZ basis set. Upon using the maug-cc-pVTZ basis set, the results for this particular case were significantly improved.

For the association reactions (**R10** and **R11**) and rearrangement reactions (**R4** and **R12**), we observe good agreement between tPBE and CASPT2 for all barriers with the exception of the reverse of reaction **R4**. In this outlier case, the error in the CASSCF reverse reaction barriers are very large, suggesting that the electron densities from the underlying CASSCF reference state subsequently used in the tPBE calculation are not sufficiently accurate, giving an inaccurate tPBE result. In contrast to CASPT2, the MC-PDFT method does not provide a first-order correction to the reference wave function, and this may explain why CASPT2 is still able to obtain an accurate result with a deficient CASSCF reference wave function.

Finally, we consider the heavy-atom transfer reactions **R5** and **R6**. The tPBE and CASPT2 results show a similar absolute error across active spaces and basis sets, but while CASPT2 often overestimates these barriers, tPBE most often underestimates these barriers. We observe a large difference in CASSCF barriers as the active space is enlarged, the resultant barrier heights become larger (more overestimated). While absolute energies decrease with increasing active space size, the product/reactant absolute energies decrease more quickly. This trend in increasing error is shadowed by the CASPT2 and tPBE results, which use CASSCF wave functions as a reference.

The distances between the atoms involved in the bond forming and bond breaking processes at each transition state geometry are given in Table 7 for the *nom*-CPO scheme and Table 8 for the *mod*-CPO scheme. Due to their abilities to capture a larger fraction of electron correlation, we expect CASPT2 and tPBE to provide improved geometries over those found using CASSCF. In order to evaluate the performance of the tPBE functional, we first compare the directions of improvement (either bond shortening or bond lengthening) relative to the CASSCF geometry for CASPT2 and tPBE for the 24 bonds listed in Tables 7 and 8. For the *nom*-CPO case, the tPBE results agree with the CASPT2 results in 17 and 19 of the 24 cases for maug-cc-pVDZ and maug-cc-pVTZ, respectively. When comparing the *mod*-CPO values, the agreement improves, with agreement in 20 of the 24 cases for both the maug-cc-pVDZ and maug-cc-pVTZ bases.

When we consider basis set effects, we find that the tPBE results are less affected than the CASPT2 ones by the basis set size. If we compare the magnitudes of how bond distances change going from maug-cc-pVDZ to maug-cc-pVTZ, we find that the average magnitude of bond distance change for tPBE is about one-half of the average magnitude of bond distance change for CASPT2. In particular, for the *nom*-CPO scheme, average magnitudes of bond distance change are 0.015 Å for tPBE and 0.030 Å for CASPT2. For the *mod*-CPO scheme, average magnitudes of bond distance change are 0.018 Å for tPBE and 0.028 Å for CASPT2. This is a similar trend to what was observed in a previous study,[34] where the tPBE functional-determined geometries were less susceptible to basis set size than CASPT2-determined geometries. We believe this to be a positive feature of the MC-PDFT methodology, as high-quality geometries can be obtained with smaller basis sets.

6. CONCLUSIONS

In this work, we have applied the MC-PDFT method to the computation of a diverse set of reaction barrier heights in the DBH24 basis set. We have demonstrated that MC-PDFT is capable of describing reaction energies and barrier heights with an accuracy very similar to what is obtained using CASPT2 but at a significantly reduced computational cost. We have shown that MC-PDFT is relatively invariant to basis set selection in comparison to CASPT2. The geometries of the stationary points found using MC-PDFT represent an improvement over the CASSCF structures. These results are quite encouraging for the application of MC-PDFT to the study of diverse chemical reactions. The accuracy of MC-PDFT for both the equilibrium and transition state regions of potential energy surfaces as well as the relatively low cost of the computation of MC-PDFT gradients should enable the use of a MC-PDFT framework for accurate and affordable dynamics computations.

■ ASSOCIATED CONTENT

Supporting Information

The Supporting Information is available free of charge on the ACS Publications website at DOI: 10.1021/acs.jpca.9b08134.

Tables of mean signed errors and mean unsigned errors (Tables S1−S5) and a complete set of geometric coordinates for each optimized species (Table S6) (PDF)

■ AUTHOR INFORMATION

Corresponding Authors

*(D.G.T.) E-mail: truhlar@umn.edu.
*(L.G.) E-mail: gagliard@umn.edu.

ORCID

Andrew M. Sand: 0000-0002-7166-2066
Katherine M. Kidder: 0000-0002-6430-4746
Donald G. Truhlar: 0000-0002-7742-7294
Laura Gagliardi: 0000-0001-5227-1396

Notes

The authors declare no competing financial interest.

■ ACKNOWLEDGMENTS

This work was supported in part by the National Science Foundation by grant no. CHE−1746186.

■ REFERENCES

(1) Karton, A. A Computational Chemist's Guide to Accurate Thermochemistry for Organic Molecules. *Wiley Interdisciplinary Reviews: Compuational Molecular Science* **2016**, *6*, 292−310.

(2) Bernardi, F.; Bottoni, A.; Olivucci, M.; Robb, M. A.; Schlegel, H. B.; Tonachini, G. Do Supra-Antara Paths Really Exist for 2 + 2 Cycloaddition Reactions? Analytical Computation of the MC-SCF Hessians for Transition States of Ethylene with Ethylene, Singlet Oxygen, and Ketene. *J. Am. Chem. Soc.* **1988**, *110*, 5993−5995.

DOI: 10.1021/acs.jpca.9b08134
J. Phys. Chem. A 2019, 123, 9809−9817

(3) Krylov, A. I.; Sherrill, C. D.; Byrd, E. F. C.; Head-Gordon, M. Size-Consistent Wave Functions for Nondynamical Correlation Energy: The Valence Active Space Optimized Orbital Coupled-Cluster Doubles Model. *J. Chem. Phys.* **1998**, *109*, 10669−10678.
(4) Szalay, P. G.; Müller, T.; Gidofalvi, G.; Lischka, H.; Shepard, R. Multiconfiguration Self-Consistent Field and Multireference Configuration Interaction Methods and Applications. *Chem. Rev.* **2012**, *112*, 108−181.
(5) Mato, J.; Gordon, M. S. Analytic Gradients for the Spin-Flip ORMAS-CI Method: Optimizing Minima, Saddle Points, and Conical Intersections. *J. Phys. Chem. A* **2019**, *123*, 1260−1272.
(6) Roos, B. O.; Taylor, P. R.; Sigbahn, P. E. M. A Complete Active Space SCF Method (CASSCF) Using a Density Matrix Formulated Super-CI Approach. *Chem. Phys.* **1980**, *48*, 157−173.
(7) Schmidt, M. W.; Gordon, M. S. The Construction and Interpretation of MCSCF Wavefunctions. *Annu. Rev. Phys. Chem.* **1998**, *49*, 233−266.
(8) Malmqvist, P.-Å.; Pierloot, K.; Shahi, A. R. M.; Cramer, C. J.; Gagliardi, L. The Restricted Active Space Followed by Second-Order Perturbation Theory Method: Theory and Application to the Study of CuO_2 and Cu_2O_2 Systems. *J. Chem. Phys.* **2008**, *128*, 204109.
(9) Ma, D.; Li Manni, G.; Gagliardi, L. The Generalized Active Space Concept in Multiconfigurational Self-Consistent Field Methods. *J. Chem. Phys.* **2011**, *135*, 044128.
(10) Odoh, S. O.; Li Manni, G.; Carlson, R. K.; Truhlar, D. G.; Gagliardi, L. Separated-pair approximation and separated-pair pair-density functional theory. *Chem. Sci.* **2016**, *7*, 2399−2413.
(11) Ghosh, S.; Cramer, C. J.; Truhlar, D. G.; Gagliardi, L. Generalized-Active-Space Pair-Density Functional Theory: An Efficient Method to Study Large, Strongly Correlated, Conjugated Systems. *Chem. Sci.* **2017**, *8*, 2741−2750.
(12) Andersson, K.; Malmqvist, P. A.; Roos, B. O.; Sadlej, A. J.; Wolinski, K. Second-order perturbation theory with a CASSCF reference function. *J. Phys. Chem.* **1990**, *94*, 5483−5488.
(13) Hirao, K. Multireference Møller-Plesset Method. *Chem. Phys. Lett.* **1992**, *190*, 374−380.
(14) Hirao, K. Multireference Møller-Plesset Perturbation Theory for High-Spin Open-Shell Systems. *Chem. Phys. Lett.* **1992**, *196*, 397−403.
(15) Hirao, K. State-Specific Multireference Møller-Plesset Perturbation Treatment for Singlet and Triplet Excited States, Ionized States and Electron Attached States of H_2O. *Chem. Phys. Lett.* **1993**, *201*, 59−66.
(16) Shavitt, I. In The Method of Configuration Interaction. *Methods of Electronic Structure Theory*; Schaefer, H. F., Ed.; Plenum: New York, 1977, 189275
(17) Shepard, R. Geometrical Energy Derivative Evaluation with MRCI Wave Functions. *Int. J. Quantum Chem.* **1987**, *31*, 33−44.
(18) Li Manni, G.; Carlson, R. K.; Luo, S.; Ma, D.; Olsen, J.; Truhlar, D. G.; Gagliardi, L. Multiconfiguration Pair-Density Functional Theory. *J. Chem. Theory Comput.* **2014**, *10*, 3669−3680.
(19) Gagliardi, L.; Truhlar, D. G.; Li Manni, G.; Carlson, R. K.; Hoyer, C. E.; Bao, J. L. Multiconfiguration Pair-Density Functional Theory: A New Way To Treat Strongly Correlated Systems. *Acc. Chem. Res.* **2017**, *50*, 66−73.
(20) Sharma, P.; Bernales, V.; Truhlar, D. G.; Gagliardi, L. Valence $\pi\pi^*$ Excitations in Benzene Studied by Multiconfiguration Pair-Density Functional Theory. *J. Phys. Chem. Lett.* **2019**, *10*, 75−81.
(21) Sharma, P.; Truhlar, D. G.; Gagliardi, L. Multiconfiguration Pair-Density Functional Theory Investigation of the Electronic Spectrum of MnO_4^-. *J. Chem. Phys.* **2018**, *148*, 124305.
(22) Presti, D.; Truhlar, D. G.; Gagliardi, L. Intramolecular Charge Transfer and Local Excitation in Organic Fluorescent Photoredox Catalysts Explained by RASCI-PDFT. *J. Phys. Chem. C* **2018**, *122*, 12061−12070.
(23) Sharma, P.; Bernales, V.; Knecht, S.; Truhlar, D. G.; Gagliardi, L. Density Matrix Renormalization Group Pair-Density Functional Theory (DMRG-PDFT): Singlet-Triplet Gaps in Polyacenes and Polyacetylenes. *Chem. Sci.* **2019**, *10*, 1716−1723.
(24) Zhou, C.; Gagliardi, L.; Truhlar, D. G. Multiconfiguration Pair-Density Functional Theory for Iron Porphyrin with CAS, RAS, and DMRG Active Spaces. *J. Phys. Chem. A* **2019**, *123*, 3389−3394.
(25) Sand, A. M.; Truhlar, D. G.; Gagliardi, L. Efficient Algorithm for Multiconfiguration Pair-Density Functional Theory with Application to the Heterolytic Dissociation Energy of Ferrocene. *J. Chem. Phys.* **2017**, *146*, 034101.
(26) Chan, G. K.-L.; Sharma, S. The Density Matrix Renormalization Group in Quantum Chemistry. *Annu. Rev. Phys. Chem.* **2011**, *62*, 465−481.
(27) Mazziotti, D. A. Two-Electron Reduced Density Matrix as the Basic Variable in Many-Electron Quantum Chemistry and Physics. *Chem. Rev.* **2012**, *112*, 244−262.
(28) Fosso-Tande, J.; Nascimento, D. R.; DePrince, A. E., III Accuracy of Two-Particle N-Representability Conditions for Describing Different Spin States and the Singlet-Triplet Gap in the Linear Acene Series. *Mol. Phys.* **2016**, *114*, 423−430.
(29) Sand, A. M.; Hoyer, C.; Truhlar, D.; Gagliardi, L. State-Interaction Pair-Density Functional Theory. *J. Chem. Phys.* **2018**, *149*, 024106.
(30) Angeli, C.; Borini, S.; Cestari, M.; Cimiraglia, R. A Quasidegenerate Formulation of the Second Order n-Electron Valence State Perturbation Theory Approach. *J. Chem. Phys.* **2004**, *121*, 4043−4049.
(31) Granovsky, A. A. Extended Multi-Configuration Quasi-Degenerate Perturbation Theory: The New Approach to Multi-State Multi-Reference Perturbation Theory. *J. Chem. Phys.* **2011**, *134*, 214113.
(32) Shiozaki, T.; Győrffy, W.; Celani, P.; Werner, H.-J. Communication: Extended multi-state complete active space second-order perturbation theory: Energy and nuclear gradients. *J. Chem. Phys.* **2011**, *135*, 081106.
(33) Yanai, T.; Saitow, M.; Xiong, X.-G.; Chalupský, J.; Kurashige, Y.; Guo, S.; Sharma, S. Multistate Complete-Active-Space Second-Order Perturbation Theory Based on Density Matrix Renormalization Group Reference States. *J. Chem. Theory Comput.* **2017**, *13*, 4829−4840.
(34) Sand, A. M.; Hoyer, C. E.; Sharkas, K.; Kidder, K. M.; Lindh, R.; Truhlar, D. G.; Gagliardi, L. Analytic Gradients for Complete Active Space Pair-Density Functional Theory. *J. Chem. Theory Comput.* **2018**, *14*, 126−138.
(35) Tishchenko, O.; Zheng, J.; Truhlar, D. G. Multireference Model Chemistries for Thermochemical Kinetics. *J. Chem. Theory Comput.* **2008**, *4*, 1208−1219.
(36) Pople, J. A. Theoretical Models for Chemistry. In *Energy, Structure, and Reactivity: Proceedings of the 1972 Boulder Summer Research Conference on Theoretical Chemistry*; Smith, D. W., McRae, W. B., Eds.; Wiley: New York, 1973; pp 51−61.
(37) Johnson, B. G.; Gill, P. M.; Pople, J. A. A Rotationally Invariant Procedure for Density Functional Calculations. *Chem. Phys. Lett.* **1994**, *220*, 377−384.
(38) Head-Gordon, M. Quantum Chemistry and Molecular Processes. *J. Phys. Chem.* **1996**, *100*, 13213−13225.
(39) Zhao, Y.; Truhlar, D. G. Assessment of Model Chemistries for Noncovalent Interactions. *J. Chem. Theory Comput.* **2006**, *2*, 1009−1018.
(40) Wang, Y.; Verma, P.; Jin, X.; Truhlar, D. G.; He, X. Revised M06 Density Functional for Main-Group and Transition-Metal Chemistry. *Proc. Natl. Acad. Sci. U. S. A.* **2018**, *115*, 10257−10262.
(41) Zheng, J.; Zhao, Y.; Truhlar, D. G. Representative Benchmark Suites for Barrier Heights of Diverse Reaction Types and Assessment of Electronic Structure Methods for Thermochemical Kinetics. *J. Chem. Theory Comput.* **2007**, *3*, 569−582.
(42) Herzberg, G. *Spectra of Diatomic Molecules*, 2nd ed.; D. Van Nostrand: Princeton, NJ, 1950; pp 540−541, 560−561.
(43) Moore, C. *National Bureau of Standards (U.S.) Circular 467*; 1952.
(44) Roberto-Neto, O.; Coitino, E. L.; Truhlar, D. G. Dual-Level Direct Dynamics Calculations of Deuterium and Carbon-13 Kinetic

DOI: 10.1021/acs.jpca.9b08134
J. Phys. Chem. A 2019, 123, 9809−9817

Isotope Effects for the Reaction Cl + CH_4. *J. Phys. Chem. A* **1998**, *102*, 4568−4578.
(45) Fdez. Galván, I.; Vacher, M.; Alavi, A.; Angeli, C.; Aquilante, F.; Autschbach, J.; Bao, J. J.; Bokarev, S. I.; Bogdanov, N. A.; Carlson, R. K.; Chibotaru, L. F.; Creutzberg, J.; Dattani, N.; Delcey, M. G.; Dong, S. S.; Dreuw, A.; Freitag, L.; Frutos, L. M.; Gagliardi, L.; Gendron, F.; Giussani, A.; Gonzalez, L.; Grell, G.; Guo, M.; Hoyer, C. E.; Johansson, M.; Keller, S.; Knecht, S.; Kovačević, G.; Källman, E.; Li Manni, G.; Lundberg, M.; Ma, Y.; Mai, S.; Malhado, J. P.; Malmqvist, P. A.; Marquetand, P.; Mewes, S. A.; Norell, J.; Olivucci, M.; Oppel, M.; Phung, Q. M.; Pierloot, K.; Plasser, F.; Reiher, M.; Sand, A. M.; Schapiro, I.; Sharma, P.; Stein, C. J.; Sørensen, L. K.; Truhlar, D. G.; Ugandi, M.; Ungur, L.; Valentini, A.; Vancoillie, S.; Veryazov, V.; Weser, O.; Wesolowski, T. A.; Widmark, P.-O.; Wouters, S.; Zech, A.; Zobel, J. P.; Lindh, R. OpenMolcas: From source code to insight. *J. Chem. Theory Comput.* **2019**, DOI: 10.1021/acs.jctc.9b00532.
(46) Papajak, E.; Leverentz, H. R.; Zheng, J.; Truhlar, D. G. Efficient Diffuse Basis Sets: cc-pVxZ+ and maug-cc-pVxZ. *J. Chem. Theory Comput.* **2009**, *5*, 1197−1202.
(47) Papajak, E.; Truhlar, D. G. Efficient Diffuse Basis Sets for Density Functional Theory. *J. Chem. Theory Comput.* **2010**, *6*, 597−601.
(48) Karton, A.; Tarnopolsky, A.; Lamère, J.-F.; Schatz, G. C.; Martin, J. M. L. Highly Accurate First-Principles Benchmark Data Sets for the Parametrization and Validation of Density Functional and Other Approximate Methods. Derivation of a Robust, Generally Applicable, Double-Hybrid Functional for Thermochemistry and Thermochemical Kinetics. *J. Phys. Chem. A* **2008**, *112*, 12868−12886.
(49) Hammond, G. S. A Correlation of Reaction Rates. *J. Am. Chem. Soc.* **1955**, *77*, 334−338.

DOI: 10.1021/acs.jpca.9b08134
J. Phys. Chem. A 2019, 123, 9809−9817